encit 2020

ABCM Associação Brasileira de Engenharia e Ciências Mecânicas

18th Brazilian Congress of Thermal Sciences and Engineering
November 16-20, 2020 (Online)

ENCIT2020-0120
MODELING AND SIMULATION OF TURBULENT FLOW OF SUPERCRITICAL CO_2 IN CENTRIFUGAL COMPRESSOR

Julia S. de Matos
Department of Mechanical Engineering, University of São Paulo, Av. Professor Mello Moraes, 2231, São Paulo, SP, Brazil
jliamatos@usp.br

Allan M. de Carvalho
Energy Engineering, Federal University of ABC, Santo André, SP, Brazil
allan.carvalho@aluno.ufabc.edu.br

Paulo E. Batista de Mello
Centro Universitário FEI, Av. Humberto de Alencar Castelo Branco, 3972, São Bernardo do Campo, SP, Brazil
pmello@fei.edu.br

Fábio Saltara
Department of Mechanical Engineering, University of São Paulo, Av. Professor Mello Moraes, 2231, São Paulo, SP, Brazil
fsaltara@usp.br

Daniel J. Dezan
Energy Engineering, Federal University of ABC, Santo André, SP, Brazil
daniel.dezan@ufabc.edu.br

Leandro Salviano
Department of Mechanical Engineering, São Paulo State University, Ilha Solteira, SP, Brazil
leandro.salviano@unesp.br

Jurandir I. Yanagihara
Department of Mechanical Engineering, University of São Paulo, Av. Professor Mello Moraes, 2231, São Paulo, SP, Brazil
jiy@usp.br

Abstract.

Computational Fluid Dynamics (CFD) has been widely used as a tool for designing, evaluating and improving turbocharger and in this context supercritical cycles have gained the scientific community's attention. This study proposes to model, simulate and evaluate the behavior of a centrifugal compressor operating with CO_2 in the thermodynamic region above the vapor-liquid critical point. In 2010, Sandia National Laboratories released a report with information regarding its small-scale Brayton cycle operating with supercritical CO_2 (S-CO_2), which has already been mainly used for validation and analysis of numerical models. To obtain accurate results of compressor's performance, fundamental aspects of flows near the critical point were investigated. Thus, a simulation model in commercial software based on a finite volume method was developed from Sandia's experimental project. The flow was numerically modeled and assumed as steady-state, turbulent and three-dimensional and only the impeller was considered. The k-ω-SST turbulence model was adopted and three meshes with different degrees of refinement were generated with later study of the mesh independence carried out by the Grid Convergence Index (GCI) method, in which low numerical uncertainties were observed. The thermodynamic properties definition was made by the generation of specific tables for the working region, used by commercial software with equations of state from Span & Wagner for S-CO_2. The results were validated in terms of pressure ratios for different cases by comparing their values with experimental ones, pointing an average mean error of 1.264%, with a maximum value of 3.012% and a minimum of 0.145%. 93.65% of the mesh elements exhibit Y+ values less than 10 and only 1.38% of the mesh elements exhibit Y+ values greater than 15. In 3D simulation, phenomenological and thermodynamic aspects were studied, in order to elucidate a greater degree of relevance of the variables related to the problem.

Keywords: *Centrifugal compressor; Supercritical CO_2; CFD; Turbulence; Compressible flow.*

1. INTRODUCTION

Despite the efforts to use renewable energy sources, such as wind and solar energy, fossil fuels continue to be the main source of energy worldwide. Therefore, alternatives for the use of process by-products and carbon emission control combined with the recent increase of exploitation and production of pre-salt basins in oil and gas production in Brazil have aroused special interest in recent years. More than 45% of known oil resources are under the see, a quarter corresponds to deep waters and 33% of world's oil production is provided by offshore plants (Barrera et al., 2015).

As a by-product of extraction, there is a gas association comprising a mixture of hydrocarbons, inert gases and water. Such a mixture requires a robust treatment and compression system, in which, once treated, hydrocarbon and CO_2-rich streams must be exported through pipelines or re-injected into reservoirs. Procedures as carbon capture and sequestration (CCS); Enhanced Oil Recovery (EOR) and supercritical power cycles are noteworthy (Ameli et al., 2017).

Carbon dioxide has a critical point around room temperature (304.2 K and 7.4 MPa), which makes this condition easy to achieve with an environmentally friendly working fluid, which makes S-CO_2 safe and inexpensive for industrial use (Wang et al., 2017). The most useful advantages of S-CO_2 are its high density, low viscosity and large pressure increase with a small increase in enthalpy, which results in a high efficiency, compact mechanical structure and a higher pressure ratio with lower input power to the centrifugal compressor.

Although notable advances have been made, a new development based on the existing turbomachinery for conventional fluids had to be developed for S-CO_2 (Ulizar & Pilidis, 2000). The importance to develop a precise numerical gas model that describes the S-CO_2 behavior and sensitivity in the performance of the turbo machine is crucial (Angelino, 1968). Therefore, since May 2008, the SANDIA National Laboratories (SNL) has had a small-scale S-CO_2 compression test loop, designed to validate models used in the design of turbomachines and heat exchangers (Wright et al., 2010). The facility was designed by SNL and Barber-Nichols Inc. and originally comprised a 50 kW motorized compressor, a gas cooler to prevent heating of the fluid along the circuit, and a valve that expands fluid to inlet pressure of the compressor.

In fact this experimental model has been used to validate models using S-CO_2 as working fluid: Pecnik et al. (2012) described a three-dimensional CFD study of a centrifugal compressor that operates with CO_2 in the thermodynamic region above the vapor-liquid critical point. A little later, Rinaldi et al. (2013) carried out a new study of the dynamics of turbo machines fluids operating with fluids characterized by a complex thermodynamic behavior. In this case, the goal was to develop a complete methodology to assist the aerodynamic design of turbo machines extended to supercritical gas turbine plants. A Group from the University of Seville has also used the SANDIAs loop facility to design a pressurized CO_2 wind model and a modular S-CO_2 design, where it is possible to analyze simple and recoverable cycles, as well as the stages of the radial compressor in independent loops (Monje, 2014).

On the present study a numeric model is validated with Sandia's compressor (Wright et al., 2010), which geometrical information is available and operational conditions have been experimentally characterized with CO_2 compression. The mesh convergence index (GCI) method is applied here in the study of mesh independence. The 3D results of the CFD for the Sandia impeller are then validated against the results of the experiments and the discussions on the respect of the flow, physical phenomena and the compressor overall performance are made.

2. METHODOLOGY

A methodology starts with CFD modeling using the finite volume method (FVM), a part of finites differences techniques and consists in solving the flow conservation equations in the differentiated control volumes that make up a continuous entire (Versteeg & Malalasekera, 2007).

For impeller's geometry and mesh generation one makes use of a specialized tool for 3D design of rotating machine components, then one builds periodical meshes domains. The grid convergence index (GCI) method following Celik et al. (2008) is applied to grid independence study. The so called RGP (real gas properties) tables are generated using an open source library for the determination of thermodynamic properties.

2.1 Governing equations

The flow was defined as three-dimensional, turbulent, and compressible at steady state. One makes use of unsteady Navier-Stokes equations in their instantaneous conservation form for continuity, momentum and total energy in a stationary frame:

$$\nabla.(\rho U) = 0 \tag{1}$$

$$\nabla.(\rho U \times U) = -\nabla \mathrm{p} + \nabla \tau + S_M \tag{2}$$

$$\nabla.(\rho U I) = \nabla.(\lambda \nabla \mathrm{T}) + \nabla.(U\tau) + U.S_M + S_e \tag{3}$$

where τ is the stress tensor. In the energy equation, the total enthalpy is dismissed and advection term uses rothalpy (I) instead. For flows in a rotating frame of reference, additional rotation sources of momentum are required (Coriolis and centrifugal forces):

$$S_M = S_{M.rot} = S_{Cor} + S_{cfg} \tag{4}$$

$$S_{cor} = -2\rho\omega \times U \tag{5}$$

$$S_{cfg} = -\rho\omega \times (\omega \times r) \tag{6}$$

and,

$$I = h_{stat} + \frac{1}{2}U^2 - \frac{1}{2}\omega^2 R^2 \tag{7}$$

Studies confirm that two equation turbulence models are the most common choice, since they are, in fact, the simplest complete model of turbulence (Wilcox, 1998). To deal with the turbulent phenomena inside the compressor, the *kω-SST* two equations turbulence model was chosen. It is, in fact, the most widespread option for industrial applications in turbo machines. This model applies the classic k-ω model to the inner part of the boundary layer and the k-ε pattern to the outer part of the boundary layer and free flow (Menter, 1994). It incorporates the transport of turbulent shear stress and provides highly accurate predictions of the onset and amount of flow separation from smooth surfaces in adverse pressure gradients. The result is a better prediction of turbulent viscosity (called Eddy viscosity), with a limitation of its value. This leads to the governing fluid flow equations and a discussion of the necessary auxiliary initial and boundary conditions.

2.2 Computational domain and boundary conditions

This study carried out an analysis of a centrifugal compressor in terms of its impeller only, since the beneficial effects of the interaction on the overall performance of the stage advance mainly in reduced blockage and slipping in the impeller, not in the diffuser itself (Shum et al., 2000). The geometry of the CO_2 centrifugal compressor of the fluid passage through the entire impeller was created using a specific software package (Fig. 1a). It calculated the periodic and symmetric geometric characteristics (Fig. 1b) and the results were extrapolated to the rest of the turbo machine, reducing the number of elements and, consequently, the computational cost. The periodic domain was treated as a rotational frame of reference, where all properties were calculated by this method and resolved with the solver.

The method for specifying the chosen inlet was parametric, so that the domain extends to the blade (main domain), independently. This ensures that the first remains stationary while the second performs the rotation movement and also avoids the problem of recirculation that occurs when fluid faces the blade. The same method of specification was chosen for the outlet, but a smallest value was chosen for the location of this domain in order to be as close to the main domain as possible, but without intersecting it, and maintaining a distance such that disturbed flows that occur at the end of the blades and do not accurately reflect the end of the flow are avoided.

The steady-state solution of the RANS equations is the result of a numerical gait method over time, so the initial conditions become very important in the speed of convergence and stability of the method. For all simulations, the turbulent intensity was defined according to the user's guide, for compressors. A normal speed component at the inlet has been adjusted for this condition. Tab. 1 summarizes the main boundary conditions applied.

Table 1: Boundary conditions applied to the flow.

Rotating speed	55000 rpm (backsweep)
Inlet total pressure	7.79 MPa
Inlet total Temperature	306.4 K
Outlet mass flow rate	2.043 kg/s
Inlet turbulence	5%
Wall condition	No-slip and adiabatic
Roughness	Smooth

There are two aspects that make S-CO_2 simulations less stable: large properties variations near the critical point and risk of condensation. These two facts require taking into account the following recommendations in order not to fail in convergence: Pressure-speed coupling adjusted with Rhie and Chow interpolation in which pressure and speed fields

are solved at the same time (non-interactive method), avoiding the uncoupling perceived in other methods. Reduce error source to obtain more accurate numerical solution, avoiding numerical dispersions. The strategy was to increase accuracy of the order of discrete approximations. Thus, for the discretization of advection terms, a high resolution scheme was used, which comprises a mix of first order upwind schemes and second order centered differences (Yeoh & Tu, 2019). A procedure based on the limit principle of Barth & Jespersen (1989) was applied to determine the proportion necessary for the assessment of advective flows. After adjusting all parameters, there is a preview of the flow development. Fig 1 (b) illustrates this scenario considering the conditions of inlet, outlet and rotational periodicity.

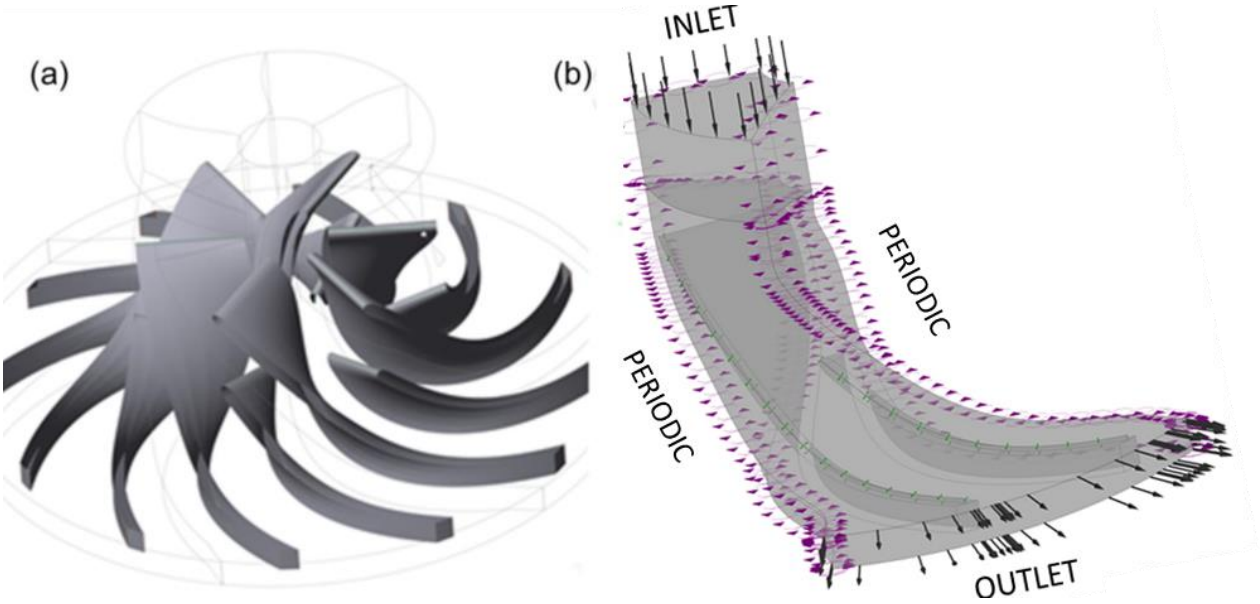

Figure 1: 3D shape of CO_2 compressor impeller (a) and the periodic computational domain with flow preview (b).

2.3 Real gas table generation

Due to the non-ideal gas behavior the CFD simulations of centrifugal compressors for S-CO_2 applications require the use of tabulated thermodynamic properties and using the real gas properties (RGP) tables, as recommended in literature. The RGP table format is described in ANSYS (2013). The file is composed by two sections called header and data. The header section contains information about the fluid (critical and triple point specification), pressure and temperature ranges and the number of points presented in a two dimension table. For this simulation a proper specification of nine superheat tables is necessary as presented in Tab 2.

Table 2: Superheat tables in data section of a RGP file.

Superheat table #	Property	Symbol
1	Specific enthalpy	h (T,P)
2	Speed of sound	c (T,P)
3	Specific volume	v (T,P)
4	Specific heat at constant volume	cv (T,P)
5	Specific heat at constant pressure	cp (T,P)
6	Partial derivative of pressure with respect to specific volume at constant temperature	$\left(\frac{\partial P}{\partial v}\right)_T$ (T,P)
7	Specific entropy	s (T,P)
8	Dynamic viscosity	μ (T,P)
9	Thermal conductivity	k (T,P)

The user enters required input parameters in the appropriate format to generate the RGP table that contains the nine necessary tables, one for each property. The name of the fluid must be informed according to program specifications, as well as the desired number of divisions for pressure and temperature (the so called table resolution), minimum and maximum pressure and temperature values and the name of the file to be generated. The first part of the superheat table shows the temperature and pressure values. Next, the property values for that table are provided. Then, the saturation temperature corresponding to each pressure value is provided, followed by the property under saturation conditions. For this study, the simulated pressure and temperature ranges are, respectively, 305.5 K and 7.676 MPa at inlet and 323K

and 10.853 MPa at outlet. A computational program was developed in C# in order to generate RGP tables in the format previously described. The fluid property is evaluated using open source library Coolprop that includes appropriate models to deal with the thermodynamic properties of gas (Bell, 2013). The program receives input parameters, demanded by the user, in the command line to generate the RGP table which contains nine necessary tables, one for each property, within it. The order of input parameters is shown in Tab 3.

Table 3: Input parameters to the computational program that generates the RGP tables.

#	Parameter
1	Fluid name, according to CoolProp specifications. It can be a mixture
2	Number of divisions in the pressure range
3	Number of divisions in the temperature range
4	Minimum pressure (in Pa)
5	Maximum pressure (in Pa)
6	Minimum temperature (in K)
7	Maximum temperature (in K)
8	Name of the RGP file to be generated (RGP extension is added by the program)

2.4 Geometrical parameters

The validation of the model presented below uses the Sandia National Laboratories (SNL) compression small scale loop facility as an experimental basis, which data are explicitly indicated in the documents by Wright et al. (2010). Additional experimental data, as well as operating conditions, are found in Meroni et al. (2018); Pecnik et al. (2013) and Vilim (2010). All together were used to generate a 3D geometric model using the commercial blading software.

The software has an Angle / Thickness operation mode which provides the design environment for the radial blades. A meridional view is used to define the blade in the radial X axial space. From this definition, the Hub and Shroud curves are generated and will be required for all other views and they are converted into Bezier curves as they are the most common option used to define these contours Casey (2012). Also in this step, the number and thickness of the blades are inserted, as well as their wrap angle. The inlet flow is assumed in the axial direction while the outflow is contained in a plane normal to the axis (purely radial machine).

Four entry angles are required for this option: β and θ, both at the entrance and at the exit to define the blades distribution angle. The value of θ is already defined as a function of the wrap angle previously defined. Therefore, only the values of β are necessary. Finally, spliters are added between the blades (50% offset) with the proper length ratio between blades and spliters chord. For both blades and spliters, trailing edge is considered cut-off, while leading edge is considered elliptical. Fig 2 (a) presents the meridional view with Hub and Shroud lines and the drawing of the impeller canal where yellow and grey lines represents respectively the fluid passage domain inlet and the out let; the orange and purple lines represent the leading edge of blades and spliters, respectively and the green line is the trailing edge of the blade, while the blue and red lines represent the Hub and Shroud, respectively. After this process, the standard geometry provided by the software is considered valid Fig. 2 (b).

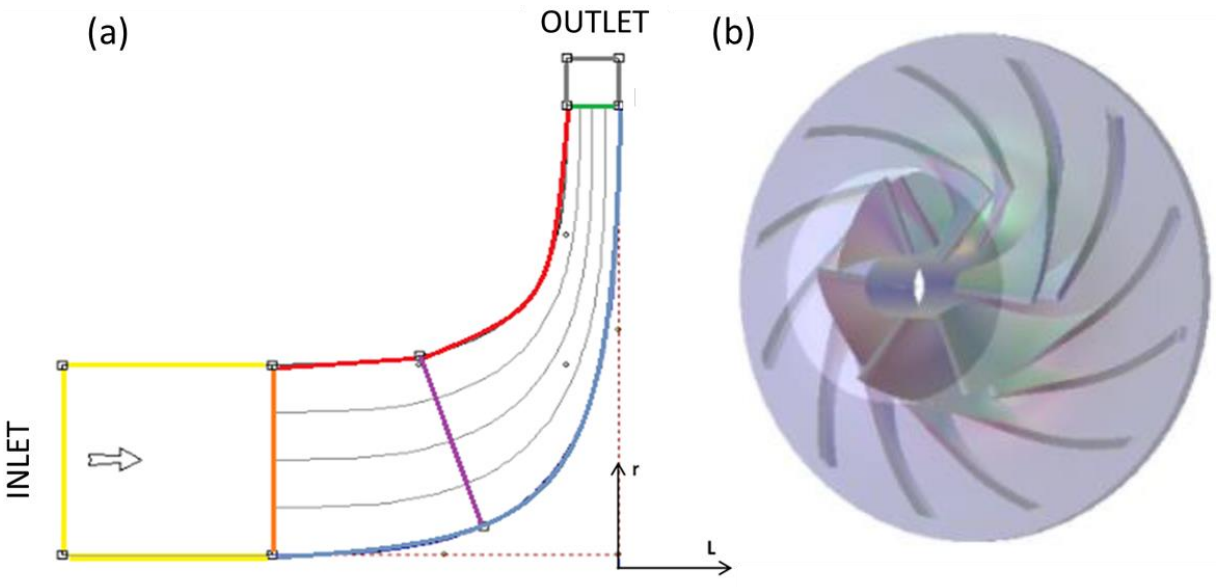

Figure 2: Meridional view of impeller canal made by Bezier curves (a) and impeller 3D final geometry (b).

2.5 Mesh generation and quality criteria

Several studies show that structured meshes are considered the most appropriate selection. The Reynolds number (based on the height of the blade) is calculated as the average value between the input and output sections. This parameter is used by the software, together with a desired *Y*+ wall, to calculate the distribution of prismatic layers in the boundary layer mesh, such that the greater the Reynolds, the smaller first layer would be for the same *Y*+ displacement. In summary, once Reynolds number has been defined, the boundary layer refinement is controlled by means of the Offset *Y*+. Again, the study presented by Monje (2014), demonstrated good results for Reynolds numbers around 10^8.

The Global Size Factor method defines the overall size of the mesh and was applied to increase the resolution of the mesh. However, the change in the overall mesh size is not linear. Thus, one can change the mesh size or the refinement of the boundary layer or do some local edge refinement on the mesh, without changing the overall size factor, however the overall mesh size may have been changed. In view of this situation, an automatic treatment close to the wall was applied. As recommended in Ansys (2013), the selection of a specific topology results from a trial and error approach, however, studies pointed out that the optimized automatic topology generally presents the best results and was, therefore, chosen. The control of the boundary layer refinement was applied using the method of proportionality to the mesh size. This option controls the number of elements within the boundary layer in proportion to base factor specified values and maintains similar expansion rates when the overall size factor is changed.

Thus, for the construction of the topology, the general parameters of the mesh were kept constant for all created meshes, while a delicate adjustment in the mesh size factor and the base factor for the boundary layer was made to achieve the desired mesh size, in order to meet the quality requirements indicated by the Software. Tab. 4 shows the specific data for each computational mesh generated.

Table 4: Generated Meshes Data.

Mesh	Coarse	Intermediate	Refined
Nº of Elements	886,440	2,032,950	4,846,402
Global Size Factor	1.168	1.4	1.83
Factor base	2.7	2.8	3.4

In terms of mesh quality, the suggestion of Ansys, (2013) follows, which takes into account the orthogonality, expansion and proportionality of the mesh. *Y* + values are also investigated. Only 5.8% of the elements have an aspect ratio above 1,000 (maximum suggested level running with double precision) and the orthogonal angle meets the suggested ranges (between 15 ° and 165 °). The complete impeller mesh is shown in Fig 3.

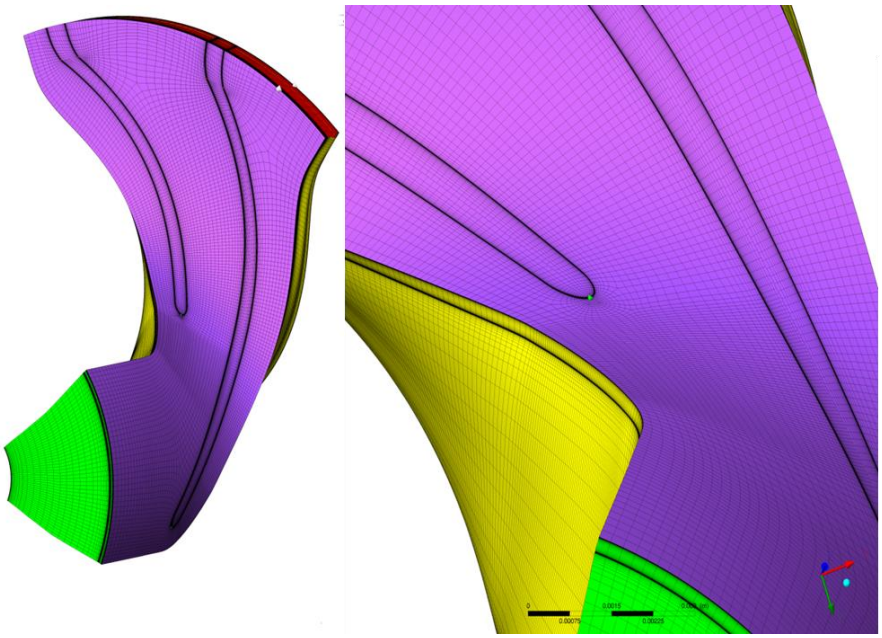

Figure 3: Meshed domain with a detailed view of the mesh at the splitter blade leading edge at the shroud.

An automatic near-wall treatment applied in regions where the value of *Y* + was greater than one. The general mesh parameters are kept constant for all created meshes while a delicate two-factor increase is implemented aiming a

progressively *Y*+ reduction. For the *Y* + values, it was observed that the majority was less than 14 in the entire domain. In fact, 93.65% of the mesh elements have *Y* + values less than 10 and occur along the blades where the flow is developed; only 1.38% of the mesh elements have *Y* + values greater than 15 and occur on the face of the trailing edge (parallel to the exit domain) of the blades. Fig. 4 shows the *Y* + values of the elements along blade and splitter.

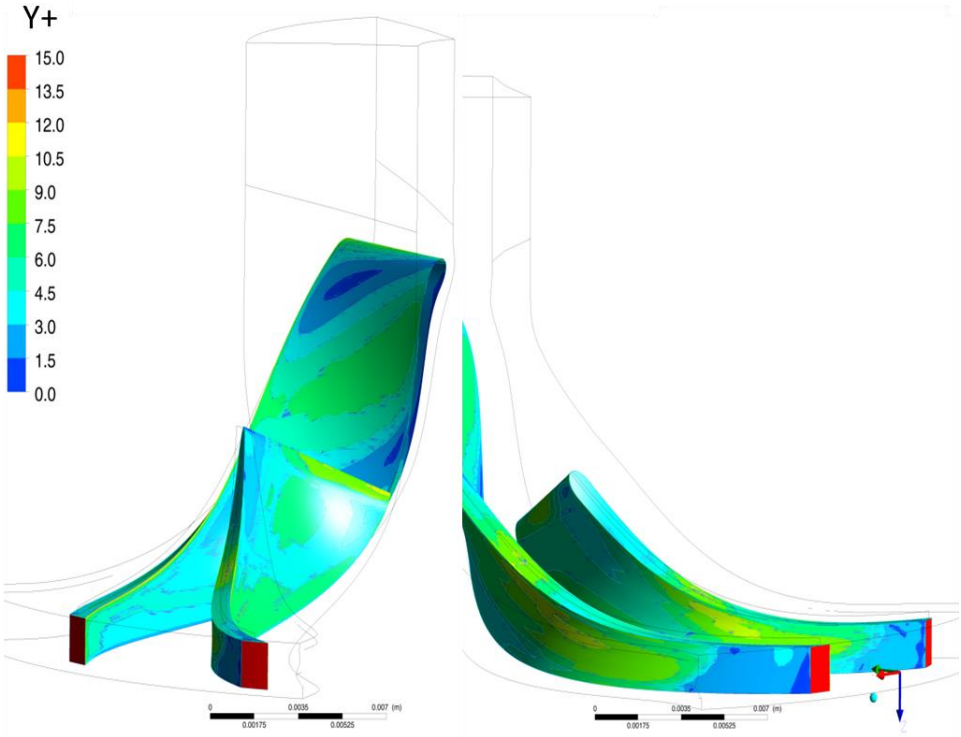

Figure 4: *Y*+ values along blade and splitter.

2.6 Grid independence study

To compare the meshes density the Grid Convergence Index (GCI) was the chosen method (Celik et al., 2008). The GCI method is based on the Richardson extrapolation (ER), estimating a value of the variable corresponding to an infinitely fine mesh and calculating the deviations of the solution obtained. The methodology requires the simulation of the same case in three different meshes with a minimum refinement rate (r) of 1.3, to which the RE is applied. This method is chosen since it is considered a robust method for studying mesh density (Celik et al., 2008).

Thus, the case presented in Tab. 1 was simulated for the three meshes the GCI method was applied. Tab. 5 summarizes the results obtained for the CGI applied to the so-called coarse, intermediate and refined meshes in terms of pressure and temperature ratios, isentropic efficiency and required power. One may concludes that numerical uncertainties are low so grid independence was reached, and the intermediate grid will be used on this research.

Table 5: Results for the GCI method.

Mesh		Coarse	Intermediate	Fine
Number of Cells		886,440	2,032,950	4,846,402
Refinement factor (r)		-	1.32	1.34
Parameter	Pressure ratio	Temperature Ratio	Isentropic Efficiency	Required Power
GCI (%)	0.00231	0.0147	0.017	0.0062

3. RESULTS AND DISCUSSION

Nine different cases were simulated and compared to the experimental results. All initial conditions of shaft speed, mass flow rate and inlet temperature and pressure as well as the experimental values where are taken from Wright et al. (2010) and are presented in Tab 6 among the results of the validation in terms of pressure ratio values for the experimental and numeric models and the relative error between them. As convergence criteria a RMS (root mean square) type residue with target value of 10^{-6} was defined for the variables of mass, momentum, energy and turbulence.

Table 6. Results of the validation for CO2 in terms of pressure ratio values and its relative error.

Case Number	N (rpm)	T01 (K)	P01 (MPa)	ṁ (kg/s)	η	PR		PR
	shaft speed	total inlet temperature	total inlet pressure	mass flow rate	isentropic efficiency	pressure ratio Exp.	Num.	relative error %
1	10000	305.50	7.676	0.4540	76.6663	1.039	1.015	2.339
2	20000	305.50	7.676	0.7710	79.7192	1.051	1.068	1.551
3	28000	305.50	7.676	1.1340	77.0515	1.112	1.125	1.156
4	39000	305.60	7.711	1.4510	74.5990	1.204	1.212	0.687
5	49000	306.30	7.854	1.8160	76.8880	1.355	1.346	0.612
6	55000	306.40	7.890	2.0430	77.9965	1.439	1.441	0.145
7	56000	306.60	7.826	2.0880	76.4763	1.469	1.449	1.385
8	60000	306.90	7.997	2.2250	76.8592	1.518	1.525	0.485
9	64900	307.90	8.211	2.4060	77.7247	1.574	1.621	3.012

There is a considerable approximation of the values obtained with the simulations: an average relative error of 1.264% with a maximum value of 3.012% and a minimum of 0.145% for the pressure ratio. In fact, the best results were observed for the case used as a basis for the design of the model and its surroundings. However, values of 2.339% and 3.012% of relative error for the cases that are most distant from the first case were considered satisfactory.

Isentropic efficiency values vary between 74.60% and 79.72%, with no specific trend as the input parameters have been changed. It is assumed that due to the small dimensions of the equipment, the results were quite susceptible to changes in the input parameters in a combined manner, since a specific parameter that dominated the effect under the efficiency values was not perceived. But in general it is pointed out that a good balance between increases in rotation speed and mass flow generated greater impact in this analysis. In general, given the complexity of the model, it can be considered suitable for its implementation.

For all run cases, pressure and temperature ranges effectively reached during the simulations remained entirely within the region covered by the RGP table used. Fig.5 illustrates the region covered by the table in light blue with upper and lower temperatures limited by lines in red and blue, respectively, as well as the effective region of the simulation for all nine cases in dark blue.

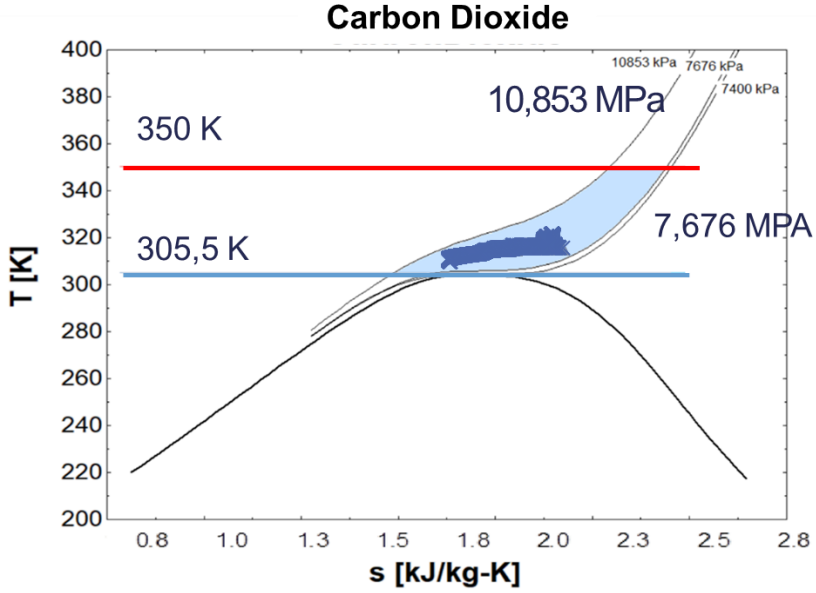

Figure 2: Region covered by the table generated for S-CO_2 and effective thermodynamic region for all nine cases.

3.1 Flow simulation analisys

When analyzing the flow velocity vectors as well as their values, one can get a sense of how it develops. Fig. 6 shows such information in 20%, 50% and 80% span for case 6 (same presented in Tab. 1). It is possible to perceive the evolution in values as the flow develops and that this profile is further intensified as it approaches the Shroud surface, where the tip clearance is found. There are small points of deceleration that recirculation occurs where the fluid hits the

blade at the leading edge until it is directed to the correct flow direction, the place of greatest speed. There are still some points of deceleration along the blade, but the flow does not block. This deceleration is all the less the closer to the Hub surface. Finally, at the exit there is a considerable increase in speed (the more pronounced the closer to the Hub surface). In general, higher velocity gradients are observed in it, with some disturbance in the velocity current lines (more pronounced the closer to the Shroud). It is also possible to see in a top view the passage of fluid between the Shroud and the top of the blade. In general, it is possible to infer that the angles applied to the blades are consistent, favoring the flow quality.

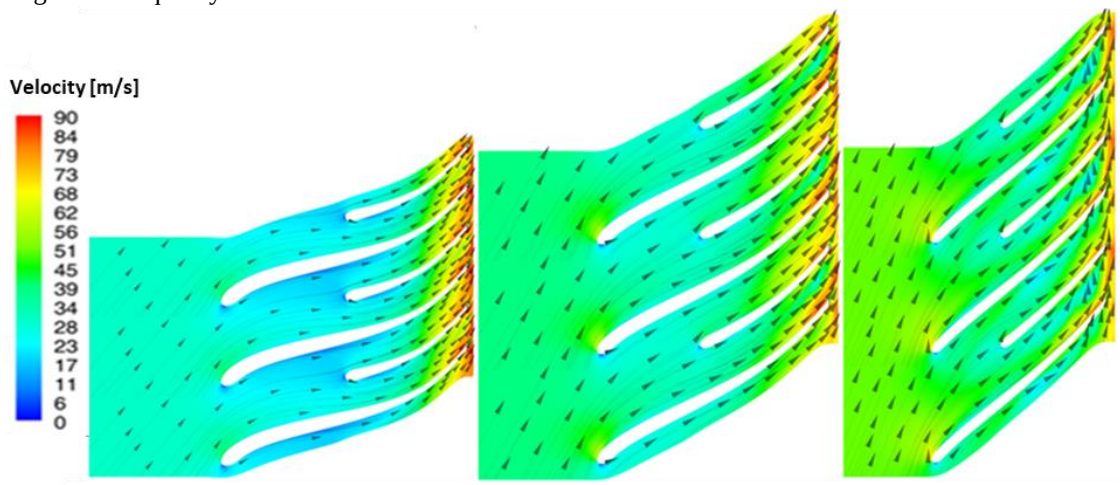

Figure 6: Scale visualization of the velocity and its vectors in the impeller for 20%, 50% and 80% span for case 6.

The two main physical phenomena that cause severe losses in centrifugal compressors are shock waves at the leading edge caused by high speeds in the blade and blockage of the flow caused by the reverse flow close to the clearance at the trailing edge. These phenomena are influenced by the blade geometry and operating conditions. When analyzing the relative Mach number along the flow in 20%, 50% and 80% Span it is possible to notice the evolution in the values as the flow develops and this profile is further intensified as it approaches the Shroud surface. Although some points have higher values at the trailing edge, their value does not exceed 0.40, therefore, there are no shock waves. There are also, at the leading edge and along the blade, some points at which the lowest relative Mach values are observed, however they do not even indicate points of stagnation or block.

In fact, the flow with greater disturbance found in the clearance on the Shroud surface (Fig 6) was a significant source of loss (since the walls were considered to be adiabatic), which can be verified by the analysis of Fig 7 of the graphical representation of entropy variation and its position along the flow. In the first half of the domain there is almost no variation in entropy, as there are only small influences of the gap. In the second half, there is the greatest variation in entropy, where the highest speeds were noticed, as well as disturbances in the current lines at the exit of the trailing edge. There is also a greater generation of entropy in the vicinity of the Hub as the speed of rotation increases.

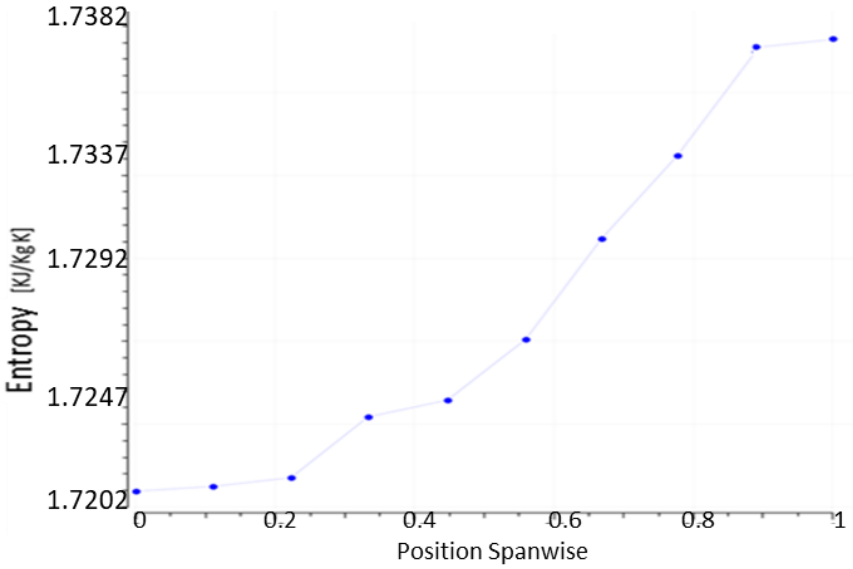

Figure 7: Entropy variation spanwise for case 6.

4. CONCLUSION

The major findings are summarized as follows: Relevant adjustments were made in the numerical model and in the thermodynamic properties using a specific table, which simulation works properly indicating that table resolution was satisfactory. Mesh independence study indicated low numerical uncertainties. The validation was made by comparing pressure ratio values for the simulation results and the experimental values. There was a considerable approximation values with an average relative error of 1.264%, maximum of 3.012% and minimum of 0.145% for the pressure ratio. The majority of $Y+$ values were less than 14 in the entire domain. 93.65% of the mesh elements have $Y+$ values less than 10 and only 1.38% of the mesh elements have $Y+$ values greater than 15. There was also an analysis of the flow in terms of the relative Mach numbers and velocity. Small deceleration points were observed with recirculation, but which did not indicate flow block. At the outlet of the fluid there is a considerable increase in speed, with some disturbance in the velocity streamlines. No Shockwaves were observed. In fact, the flow with the most disturbances was a significant source of loss that can be seen in terms of static entropy along the flow. In general, given the complexity of the model, it can be considered suitable for implementation in a design and optimization tool to be used in the operation of supercritical carbon dioxide.

5. REFERENCES

Ameli, Alireza et al. Numerical Sensitivity Analysis for Supercritical CO2 Radial Turbine Performance and Flow Field. Energy Procedia, v. 129, p. 1117-1124, 2017.

Angelino, G. Carbon Dioxide Condensation Cycles For Power Production. Journal of Engineering for Power, 90(3), 287–295, 1968.

ANSYS, CFX. ANSYS TurboSystem User's Guide, Release 15.0, 2013.

Barrera, J. E., Bazzo, E., & Kami, E. Exergy analysis and energy improvement of a Brazilian floating oil platform using Organic Rankine Cycles. Energy, 88, 67–79, 2015.

Barth, T., & Jespersen, D.. The design and application of upwind schemes on unstructured meshes. In 27th Aerospace Sciences Meeting. American Institute of Aeronautics and Astronautics, 1989.

Bell, Ian H. et al. Coolprop: An open-source reference-quality thermophysical property library. In: ASME ORC 2nd International Seminar on ORC Power Systems, 2013.

Casey, M. Robinson, C., Hutchinson, B., & Steed, R. Impeller-diffuser interaction in centrifugal compressors. Proceedings of the ASME Turbo Expo, 8(PARTS A, B, AND C), 767–777, 2012.

Celik, I.B.; Ghia, U.; Roache, P.J.; Freitas, C.J.; Coleman, P.E. Raad, Procedure for Estimation and Reporting of Uncertainty Due to Discretization in CFD Applications, J. Fluids Eng. 130, 1–4, 2008.

Menter, F. R. Two-equation eddy-viscosity turbulence models for engineering applications. AIAA Journal, 32(8), 1598–1605, 1994.

Meroni, Andrea et al. Design of centrifugal compressors for heat pump systems. Applied energy, v. 232, p. 139-156, 2018.

Monje, Benjamin Brenes. Design of supercritical carbon dioxide centrifugal compressors. PHD Thesis. Universidad de Sevilla, 2014.

Pecnik, R., Rinaldi, E., & Colonna, P. Computational Fluid Dynamics of a Radial Compressor Operating With Supercritical CO2. Journal of Engineering for Gas Turbines and Power, 134, 122301, 2012.

Pecnik, R., Rinaldi, E. & Colonna, P. Computational Fluid Dynamics of a radial compressor operating with supercritical CO2. Copenhagen (Denmark), Paper NO.GT2012-69640, Proceedings of ASME Turbo Expo, 2013.

Rinaldi, E.; Pecnik, R & Colonna, P. Steady state CFD investigation of a radial compressor operating with supercritical CO2. ASME Paper No. GT2013-94580, 2013.

Shum, Y. K. P., Tan, C. S., & Cumpsty, N. A. Impeller–Diffuser Interaction in a Centrifugal Compressor . Journal of Turbomachinery, 122(4), 777–786, 2000.

Ulizar, I., & Pilidis, P. Handling of a Semiclosed Cycle Gas Turbine With a Carbon Dioxide-Argon Working Fluid . Journal of Engineering for Gas Turbines and Power, 122(3), 437–441, 2000.

Versteeg, Henk Kaarle & Malalasekera, Weeratunge. An introduction to computational fluid dynamics: the finite volume method. Pearson Education, 2007.

Vilim, R. B. A One-Dimensional Compressor Model for Super-Critical Carbon Dioxide Applications. International Congress, Advances in Nuclear Power Plants, 3, 1581–1591, 2010.

Wang, Y., Shi, D., Zhang, D., & Xie, Y. Investigation on Unsteady Flow Characteristics of a SCO2 Centrifugal Compressor. Applied Sciences, 7, 310, 2017.

Wilcox, D. C. Turbulence modeling for CFD (Vol. 2). DCW industries La Canada, CA, 1998.

Wright, S. A., Radel, R. F., Vernon, M. E., Rochau, G. E., & Pickard, P. S. Operation and Analysis of a Supercritical CO 2 Brayton Cycle. September, 2010.

Yeoh, G. H., & Tu, J. Chapter 2 - Governing Equations and Boundary Conditions (G. H. Yeoh & J. B. T.-C. T. for M. F. (Second E. Tu (Eds.); pp. 19–83). Butterworth-Heinemann, 2019.